

# Mind the Gap: Learning Implicit Impedance in Visuomotor Policies via Intent-Execution Mismatch

Cuijie Xu<sup>1</sup>, Shurui Zheng<sup>1,2</sup>, Zihao Su<sup>3</sup>, Yuanfan Xu<sup>1</sup>,  
 Tinghao Yi<sup>4</sup>, Xudong Zhang<sup>1</sup>, Jian Wang<sup>1</sup>, Yu Wang<sup>1</sup>, Jinchen Yu<sup>1\*</sup>

<sup>1</sup>Department of Electronic Engineering, Tsinghua University

<sup>2</sup>Qiuzhen College, Tsinghua University

<sup>3</sup>School of Mechanical and Aerospace Engineering, Jilin University

<sup>4</sup>EFORT Intelligent Robot Co., Ltd.

\*Email: yu-jc@mail.tsinghua.edu.cn

**Abstract**—Teleoperation inherently relies on the human operator acting as a closed-loop controller to actively compensate for hardware imperfections, including latency, mechanical friction, and lack of explicit force feedback. Standard Behavior Cloning (BC), by mimicking the robot’s executed trajectory, fundamentally ignores this compensatory mechanism. We argue that this omission is fatal on the low-cost, sensorless hardware, where the significant divergence between “command” and “execution” causes standard policies to fail. In this work, we propose a Dual-State Conditioning framework that shifts the learning objective to “Intent Cloning” (master command). We posit that the Intent-Execution Mismatch—the discrepancy between master command and slave response—is not noise, but a critical signal that physically encodes implicit interaction forces and algorithmically reveals the operator’s strategy for overcoming system dynamics. By predicting the master intent, our policy learns to generate a “virtual equilibrium point”, effectively realizing implicit impedance control. Furthermore, by explicitly conditioning on the history of this mismatch, the model performs implicit system identification, perceiving tracking errors as external forces to close the control loop. To bridge the temporal gap caused by inference latency, we further formulate the policy as a trajectory inpainter to ensure continuous control. We validate our approach on a sensorless, low-cost bi-manual setup. Empirical results across tasks requiring contact-rich manipulation and dynamic tracking reveal a decisive gap: while standard execution-cloning fails due to the inability to overcome contact stiffness and tracking lag, our mismatch-aware approach achieves robust success. This presents a minimalist behavior cloning framework for low-cost hardware, enabling force perception and dynamic compensation without relying on explicit force sensing. Videos are available on the project page.

## I. INTRODUCTION

The widespread application of robots requires low-cost and highly reliable hardware. However, a significant gap remains: while humans can perform delicate tasks using imperfect interfaces—compensating for communication latency, mechanical backlash, and friction through adaptive control—robots typically require expensive, high-fidelity hardware (e.g., torque and tactile sensors) to achieve similar compliance.

In this work, we ask: Can we bridge this gap by **learning the human’s compensatory strategy directly from data, enabling precise manipulation on sensorless, imperfect hardware?**

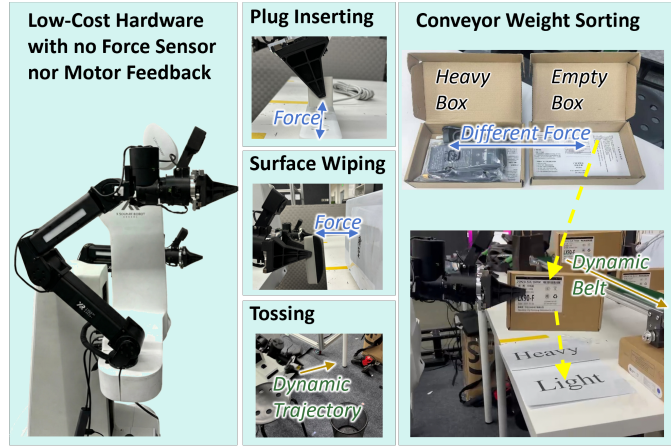


**Fig. 1: Implicit Impedance Learning on Sensorless Hardware.** Our method enables low-cost, position-controlled robots (left) to master force-sensitive and dynamic tasks without explicit force, tactile, or motor current feedback. By conditioning on the “Intent-Execution Mismatch”, the policy successfully performs tasks such as: high-precision plug insertion, force-modulated surface wiping, dynamic tossing, and proprioceptive weight sorting of visually identical objects.

Achieving robust control in contact-rich scenarios has traditionally relied on high-fidelity hardware equipped with precision sensing capabilities. While recent advances in generative models, such as Diffusion Policies [6] and Transformers [25], have enabled remarkable generalization in free-space motion, they often fail when deployed on low-cost sensorless systems in contact-rich tasks. Without the direct feedback provided by expensive torque or tactile transducers, standard policies exhibit brittleness in tasks requiring precise force regulation, such as precision assembly or dynamic handling, where success depends on physical interaction rather than mere trajectory tracking [21].

From an algorithmic perspective, handling these contact dy-

namics typically necessitates explicit force feedback loops and analytical impedance control frameworks. On the perception side, this paradigm often demands expensive, high-precision force-torque sensors; sensorless alternatives typically rely on motor current monitoring coupled with complex analytical modeling to compensate for gravity and friction, rendering them sensitive to calibration errors. On the control side, variable impedance approaches require explicitly estimating stiffness parameters and modeling virtual equilibrium points. Consequently, these pipelines are often cumbersome to tune and difficult to integrate seamlessly into pixel-to-action learning policies.

Beyond interaction dynamics, the inference latency of foundation models introduces a critical consistency challenge that exacerbates covariate shift. While offline training data typically consists of smooth, synchronous state-action trajectories, online deployment suffers from computational delays that disrupt the continuity of control signals. This creates a fundamental training-inference mismatch: for policies relying on historical context, the effective history buffer during inference becomes “stale” or discontinuous, diverging significantly from the ground-truth sequences seen during training. This distribution shift is particularly detrimental in high-precision tasks, where the model—blind to these temporal gaps—predicts actions based on drifted history, leading to compounding errors and eventual control failure.

In this work, we propose a minimalist, data-driven alternative that bypasses these explicit hardware, modeling, and timing constraints. We argue that the fragility of current learning methods stems from a fundamental misconception in how “observation” and “action” is defined. In teleoperation, the human operator acts as a high-level controller, actively compensating for environmental stiffness and hardware latency by commanding the master interface to positions that deviate from the robot’s actual execution.

In standard Behavior Cloning (BC), the prevailing practice is to clone the robot’s measured state (slave state), which we term “Execution Cloning”, both the input and output is slave state (S2S). While intuitive, this approach discards the compensatory signal inherent in the operator’s command, resulting in a force-agnostic policy incapable of generating necessary contact forces. Recent works like ALOHA [25] have noted the utility of predicting leader (master) joint positions. However, this is often treated as a heuristic implementation detail. We elevate this to a rigorous framework, deconstructing the role of “Intent” (Master) versus “Execution” (Slave) through two mechanisms: Force Generation and Force Perception.

We introduce Dual-State Conditioning (SM2M, Slave and Master as input & Master as output), which explicitly conditions on this mismatch, allowing the network to perceive tracking errors as external forces and dynamically compensate for disturbances (e.g., stiction or tracking lag). In summary, our contributions are:

- **Mechanistic Deconstruction of Intent:** We systematically analyze the physical role of action spaces, identifying *Intent Cloning* (master output) as the prerequisite

for implicit force generation and *Dual-State Conditioning* (master and slave input) as the mechanism for closed-loop force perception.

- **Latency-Adaptive Inpainting Policy:** We reformulate trajectory prediction as a *conditional sequence inpainting* task, employing explicit validity masks to dynamically adapt to varying inference delays and ensure consistent control flow.
- **Broad Empirical Validation:** We validate the universality of our framework by instantiating it across diverse backbone architectures, including Diffusion Policy [6] and  $\pi_0$  [2]. Through extensive experiments ranging from contact-rich to dynamic manipulation, we demonstrate that our approach consistently achieves robust control on sensorless hardware.

With the help of SM2M, the sensorless robot can learn the human’s compensatory strategy as the implicit impedance. As shown in Fig. 1, the sensorless robot can perform challenging force-sensitive tasks such as plug inserting, surface wiping, tossing and the conveyor weight sorting, distinguishing the empty box.

## II. RELATED WORK

### A. Visuomotor Imitation Learning and Action Representations

Visuomotor learning has evolved from simple behavioral cloning to modeling complex, multimodal distributions. Generative models currently dominate this landscape: ACT [25] utilizes CVAEs to chunk actions, while Diffusion Policies [6] and their accelerated variants like Consistency Policy [15] employ denoising processes to capture high-precision continuous behaviors. Parallel research explores discrete representations, such as BeT [19] and VQ-BeT [13], framing control as sequence modeling with GPT-style Transformers. On the scale front, foundational models like RT-2 [3], Octo [20], and RT-X [8] demonstrate generalization across heterogeneous embodiments by leveraging massive datasets. Despite these advancements, standard methods predominantly perform “Execution Cloning” ( $q_{measured}$ ). By strictly mimicking the robot’s executed trajectory, these approaches often fail to capture the operator’s underlying intent, rendering policies brittle under physical disturbances or hardware imperfections.

### B. Learning Compliance and Force Perception without Sensors

Contact-rich manipulation, such as assembly, inherently requires regulating interaction forces. Classically, this is addressed via Impedance Control. In the learning domain, recent works have attempted to bridge this gap by encoding compliance. ResiP [1] proposes learning a residual policy to modulate stiff trajectories, while RDP [22] and ImplicitRDP [5] introduce explicit force encoding or dual-stream architectures to handle contact dynamics. Similarly, Geiger et al. [11] present a diffusion-based approach for learning impedance parameters that adapts robustly to contact-rich environments. ForceVLA

[23] further enhances vision-language-action models by integrating a force-aware Mixture-of-Experts module tailored for contact-rich manipulation.

However, relying on explicit force sensors increases hardware cost. While adaptive methods like RMA [12] utilize trajectory history for system identification, they often assume reliable motor feedback. On low-cost hardware, motor-current-based estimation [24] is often noisy due to friction. Our work proposes a sensorless alternative. We posit that the Intent-Execution Mismatch serves as a high-fidelity proxy for interaction force ( $F \propto q_{master} - q_{slave}$ ). Unlike methods that treat tracking error as a defect, we explicitly condition our policy on this mismatch, enabling force modulation purely through position encoders.

### C. Bilateral Control and Intent-Aware Architectures

The utility of separating Master (command) and Slave (response) states is rooted in Bilateral Teleoperation. In imitation learning, early works [21, 18] demonstrated that predicting the Master’s command inherently compensates for system latency and reaction forces. This concept has recently been integrated with Transformer architectures in Bi-ACT [10] and torque-based controllers in IL-BiT [14]. Simultaneously, the rise of low-cost, human-centric interfaces like Mobile ALOHA [9], AnyTeleop [16], and UMI [7] highlights the importance of capturing high-frequency human intent. Our work bridges these domains. Unlike prior bilateral methods that often focus on specific force-feedback hardware, we propose a general Dual-State Conditioning framework for sensorless robots. Treating control as a sequence modeling problem [4], we formulate the policy to predict future master intentions, leveraging the mismatch to realize implicit impedance control and robustly bridge the inference latency gap.

## III. METHODOLOGY

### A. Problem Formulation: Learning Implicit Impedance via Inverse Dynamics

We formalize the visuomotor control problem in the task space. Let  $\mathbf{x}_t^s \in SE(3)$  denote the *Slave (Execution)* pose and  $\mathbf{x}_t^m \in SE(3)$  denote the *Master (Intent)* pose.

**Dynamics of the Black-Box Controller.** In low-cost or compliant robotic setups, the relationship between the commanded intent and the actual execution is non-identity. We model the low-level control stack (encompassing IK, PID, latency, and environmental contact) as a dynamic *Black Box* function  $\mathcal{B}$  with varying internal parameters  $\theta_{env}$ :

$$\mathbf{x}_{t+1}^s = \mathcal{B}(\mathbf{x}_t^s, \mathbf{x}_t^m; \theta_{env}) \quad (1)$$

This generalized model captures various system discrepancies driven by  $\theta_{env}$ :

- **Stiffness:** In rigid contact,  $\mathbf{x}^s$  lags behind  $\mathbf{x}^m$  due to finite controller gains.
- **Latency:** In high-speed motion,  $\mathbf{x}^s$  lags temporally behind  $\mathbf{x}^m$  due to communication or processing delays.
- **Friction:** Small changes in  $\mathbf{x}^m$  may yield zero change in  $\mathbf{x}^s$  until a “break-away” threshold is reached.

- **Gravity:** Lacking ideal gravity compensation,  $\mathbf{x}^s$  maintains a static vertical offset below  $\mathbf{x}^m$  to generate the necessary holding torque against gravity.

**The Human as an Inverse Controller.** Crucially, standard teleoperation data is not merely a record of desired trajectories; it is a trace of a human operator actively closing the loop around  $\mathcal{B}$ . To achieve a desired object motion  $\mathbf{x}^{des}$ , the operator internally approximates the *Inverse Dynamics*  $\mathcal{B}^{-1}$  and generates a *compensatory intent*  $\mathbf{x}^m$ :

$$\mathbf{x}_t^m \approx \mathcal{B}^{-1}(\mathbf{x}_{t+1}^{des}, \mathbf{x}_t^s; \theta_{env}) \quad (2)$$

For example, to compensate for latency, the human leads the target (Feedforward); to compensate for contact stiffness, the human commands a virtual penetration (Implicit Impedance). The *Intent-Execution Mismatch*  $\epsilon_t = \mathbf{x}_t^m \ominus \mathbf{x}_t^s$  effectively encodes this compensatory control signal.

**The Monotonic Impedance Assumption.** While  $\mathcal{B}$  is complex, for the specific purpose of learning manipulation, we rely on a fundamental property of stable feedback controllers: *Monotonicity*. We model the external interaction wrench  $\mathbf{F}_{ext} \in \mathbb{R}^6$  (force and torque) as a function of the mismatch:

$$\mathbf{F}_{ext} \approx \mathcal{F}(\epsilon_t, \mathbf{x}_t^s) \quad (3)$$

We assume  $\mathcal{F}$  satisfies:

- Directional Alignment:  $\epsilon_t^\top \mathbf{F}_{ext} < 0$ .
- Magnitude Correlation: Larger mismatch  $\|\epsilon_t\|$  induces larger force  $\|\mathbf{F}_{ext}\|$  (up to saturation).

This assumption ensures that even without an analytical model of  $\mathcal{B}$ , the mismatch  $\epsilon_t$  serves as a **valid proxy for force**. Crucially, this monotonic relationship is valid within a safe operating range  $\|\epsilon_t\| < \delta_{max}$ . Beyond this threshold, low-level hardware safety protocols (e.g., motor current limits) trigger a protective stop.

**Deconstructing Learning Objectives.** As shown in Fig. 2, in the teleoperation stage of Imitation Learning, the  $\mathbf{x}^m$  and  $\mathbf{x}^s$  are recorded as training data. In policy learning stage, the goal of Imitation Learning is to recover this inverse policy  $\mathbf{x}_{t+1} = \pi(O)$ , Where  $O$  is the observation including the image ( $I_t$ ) and the state ( $\mathbf{x}_t$ ). In deployment stage, the expected action  $A$ , namely  $\mathbf{x}^m$  or  $\mathbf{x}^s$ , is executed as  $\hat{A}$  through a non-ideal controller. This formulation reveals why standard approaches fail and necessitates our Dual-State framework:

a) *The Failure of Execution Cloning (S2S):* S2S minimizes the divergence between the policy output and the robot’s realized state ( $\pi(\cdot) \approx \mathbf{x}^s$ ). Ideally, manipulation involves solving the *Inverse Dynamics* to generate a command  $\mathbf{x}^m$  that produces the desired motion under external forces  $\mathbf{F}_{ext}$ . However, S2S effectively treats the black-box controller  $\mathcal{B}$  as an identity function ( $\mathbf{x}^s \approx \mathbf{x}^m$ ). This assumption discards the implicit control signal required to generate interaction forces. Consequently, the learned policy becomes *force-agnostic*: it learns to satisfy geometric constraints (e.g., stopping at surface contact) but fails to encode the *virtual penetration* necessary to exert force against environmental stiffness.

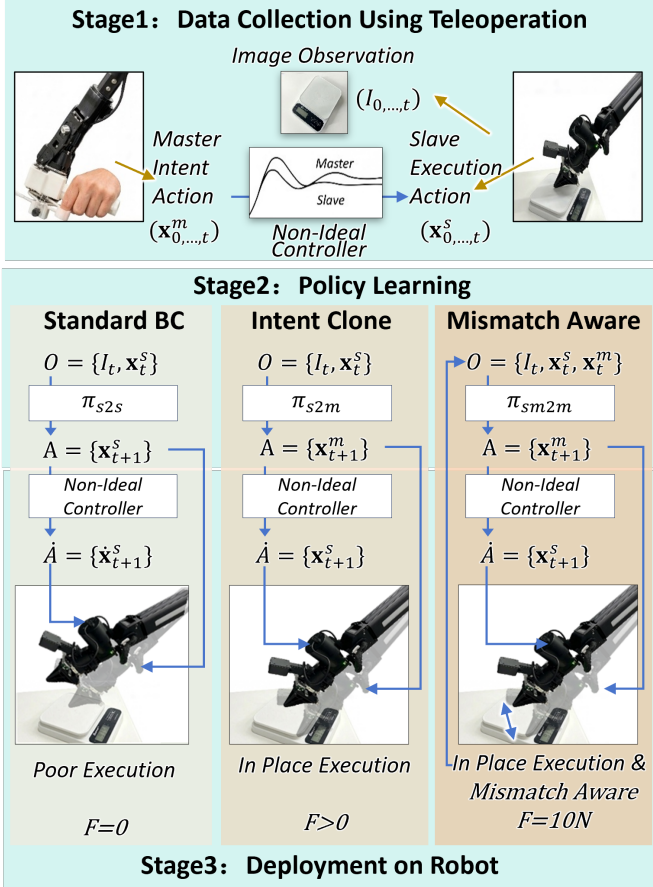


Fig. 2: In teleoperation stage, the human operator acts as an inverse controller, compensating for hardware limitations (the “black box non-ideal controller”) by commanding a Master Intent that deviates from the Slave Execution. **Standard behavior cloning (BC, S2S):** Due to non-ideal controller, the expected output slave action ( $A = X^s$ ) is poorly executed as  $\hat{A} = \dot{X}^s$ . **Force Generation via Inverse Dynamics (S2M):** By cloning the Master Intent, the policy learns a Virtual Equilibrium Point that penetrates constraints ( $A = X^m$ ) and executed as the expected out  $\hat{A} = X^s$  through the non-ideal controller. **Force Perception via System ID (SM2M):** By explicitly conditioning on the Intent-Execution Mismatch, the policy performs implicit system identification to recover the closed-loop feedback needed to adapt to dynamic uncertainties.

*b) Mechanism 1: Force Generation via Intent (S2M):*

This corresponds to learning the *Static Inverse Dynamics*. By predicting  $x^m$ , the policy learns to output a *Virtual Equilibrium Point* that penetrates constraints. Physically, this exploits the *Monotonicity* property to generate a desired interaction force. However, without history, S2M assumes a fixed environment  $\theta_{env}$ , making it an open-loop force generator liable to failure under dynamic variations.

*c) Mechanism 2: Force Perception via Implicit System ID (SM2M):* This corresponds to *Closed-Loop Adaptation*.

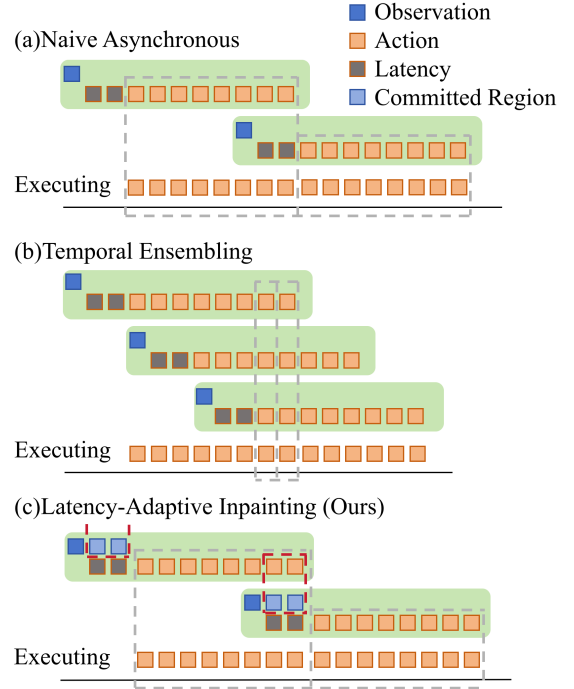


Fig. 3: Comparison of asynchronous control pipelines. (a) Naïve Asynchronous Streaming, where immediate switching causes kinematic jumps. (b) Temporal Ensembling, which averages overlapping predictions to smooth transitions but introduces reaction lag by aggregating actions based on stale observations. (c) Our Latency-Adaptive Inpainting (Ours), which conditions generation on the committed buffer to enforce continuity while maintaining immediate reactivity to the latest observation.

While the function  $\mathcal{B}$  is unknown, the mismatch sequence  $(x^m_{t-H:t}, x^s_{t-H:t})$  contains sufficient statistics to infer the local system parameters  $\hat{\theta}_{env}$  (e.g., distinguishing “hitting a wall” from “moving in free space”). We term this *Implicit System Identification*. By conditioning on this signal, SM2M aligns the policy’s observation space with the human operator’s, allowing it to perceive tracking errors as external forces and dynamically adjust the *Virtual Equilibrium Point* to compensate for disturbances.

### B. Latency-Adaptive Control via Sequence Inpainting

While shifting the action space to *Intent* (Section 3.1) solves the physical interaction gap, deploying such policies on high-capacity backbones (e.g., VLAs) introduces a significant *temporal gap*: the inference latency ( $\delta_{inf}$ ) often exceeds the control period ( $\Delta t$ ), breaking the closed-loop stability required for high-frequency contact. Standard approaches typically rely on rigid “Action Chunking” [25], as shown in Fig. 3 (a), which locks the robot into a fixed trajectory for a set horizon, reducing reactivity.

To bridge this gap without sacrificing model capacity, we reformulate the trajectory generation problem as a *Conditional Sequence Inpainting* task, as shown in Fig. 3 (c). This

paradigm treats the “future intent” as a partially observable sequence, where the initial segment is constrained by the system’s latency and the remaining segment is generated by the policy.

**Intent Buffering and Explicit Masking.** We define the target intent sequence at time step  $t$  as  $\mathbf{X}_{t+1:t+H}^m = \{\mathbf{x}_{t+1}^m, \dots, \mathbf{x}_{t+H}^m\}$ . Due to inference latency, by the time the policy finishes computing at  $t + \delta_{inf}$ , the robot has already executed the first  $k = \lceil \delta_{inf}/\Delta t \rceil$  steps of the previous plan. These  $k$  steps are now immutable history (or “committed intent”).

To model this, we introduce *Explicit Validity Mask*  $\mathbf{M} \in \{0, 1\}^H$ .

- **Committed Region** ( $m_i = 1$ ): For steps  $i \leq k$ , the trajectory is fixed to the previously generated intent buffer. The policy must condition on these steps to ensure  $C^1$  continuity (velocity smoothness) at the handover point.
- **Inpainting Region** ( $m_i = 0$ ): For steps  $i > k$ , the trajectory is unknown. The policy must “inpaint” these steps based on the latest visual observation  $I_t$  and proprioceptive mismatch  $\epsilon_t$ .

The input to the policy  $\pi$  becomes a tuple:  $(\mathbf{X}_{t:t+H}^m, \mathbf{M}, \mathbf{x}_t^s, I_t)$ , where  $\mathbf{X}_{t:t+H}^m$  contains valid values only where  $\mathbf{M} = 1$ .

Implementation-wise, this masking strategy is architecture-agnostic. For Transformer-based policies, it is naturally implemented via the causal attention mask preventing information leakage from the unknown future. For UNet-based diffusion policies [6], the mask and the committed trajectory are typically concatenated as additional input dimensions.

**Randomized Context Training.** A key innovation of our framework is *Elasticity*: the ability to adapt to varying latencies at runtime (e.g., fluctuating GPU loads or different hardware platforms). To achieve this, we employ *Randomized Context Training*. During training, we do not fix the mask length  $k$ . Instead, we sample  $k \sim \mathcal{U}[0, K_{max}]$  for each sample.

**Inference: Elastic Streaming.** At inference time, we dynamically measure the real-time latency  $\delta_{inf}$ .

- 1) We calculate the required committed horizon  $k_{curr} = \lceil \delta_{inf}/\Delta t \rceil$ .
- 2) We construct the mask  $\mathbf{M}$  with the first  $k_{curr}$  bits set to 1.
- 3) The policy inpaints the rest of the sequence starting precisely from the end of the committed buffer.

This mechanism effectively decouples the control frequency (which depends on the buffer execution rate) from the inference frequency (which depends on model speed). Unlike standard asynchronous wrappers that simply overwrite old trajectories (causing jumps), our inpainting formulation mathematically guarantees that the new intent smoothly extends the currently executing intent, maintaining the stability of the implicit impedance controller even under jittery latency conditions.

## IV. EXPERIMENT

Our proposed framework serves as a minimalist yet effective modification to standard imitation learning, applicable to diverse teleoperation interfaces—ranging from bilateral master-slave arms to VR controllers and spatial mice—and compatible with various policy backbones. To rigorously validate its universality and robustness, we conduct extensive real-world experiments designed to investigate the following research questions:

- **Q1 Validation of Monotonic Impedance:** Does the proposed *Intent-Execution Mismatch* signal serve as a valid, monotonic proxy for physical interaction forces on sensorless hardware?
- **Q2 Force Generation:** Can *Intent Cloning* (S2M) effectively generate the implicit impedance required for contact-rich tasks, where standard Execution Cloning (S2S) fails?
- **Q3 Force Perception:** Does *Dual-State Conditioning* (SM2M) enable the policy to perceive the magnitude of the force, thereby improving the success rate?
- **Q4 Latency Robustness:** Can our *Latency-Adaptive Inpainting* mechanism maintain smooth, successful control under varying and significant inference delays?

Due to space constraints, we provide comprehensive reproducibility details in the Supplementary Material. This includes: (1) architectural modifications for adapting DP and  $\pi_0$ ; (2) hyperparameter and dataset statistics for all tasks; and (3) qualitative results, including video demonstrations of policy rollouts and a detailed analysis of failure modes.

### A. Setup

1) *Hardware Configuration:* We evaluate our framework on a low-cost bi-manual teleoperation suite consisting of two ARX-R5 (Slave) and ARX-X5 (Master) 6-DoF robotic arms. The system operates at a control frequency of 60Hz. Crucially, to validate the strictly sensorless nature of our approach, we intentionally exclude motor current readings from the policy input. This design choice highlights that our Intent-Execution Mismatch signal serves as a sufficient and cleaner proxy for interaction forces, eliminating the need for the complex gravity compensation or system identification typically required to extract useful force information from noisy motor currents. Visual observations are provided by two wrist-mounted RGB camera and a first-person RGB camera streaming at 20Hz.

2) *Task Suite:* We design a suite of six tasks to isolate and evaluate specific manipulation capabilities, ranging from force generation, force perception to dynamic motion compensation.

- **Microwave Manipulation Sequence.** This long-horizon task requires the robot to open a microwave door, grasp an object from a side plate, place it inside the microwave, and close the door. The primary bottleneck is the mechanical push-button (Fig. 4 (a)) mechanism: opening the door requires firmly pressing a stiff button ( $\approx 10\text{N}$ ) to release the latch.

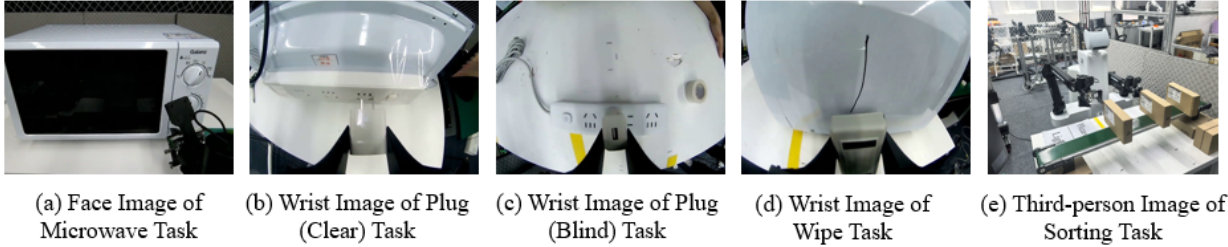


Fig. 4: Overview of the manipulation tasks.

- **Plug Insertion (Clear).** The robot must insert a standard two-prong plug into a fixed electrical socket. As shown in Fig. 4 (b), both the plug pins and socket holes are fully visible. The challenge lies in the tight geometric tolerances. Success requires the policy to maintain a stiff grasp to push through friction while remaining compliant enough to resolve minor misalignments.
- **Plug Insertion (Blind).** Similar to the task above, but the socket holes are visually occluded by the plug, as shown in Fig. 4 (c). The policy must rely on the proprioceptive feedback to perform a local search, distinguishing between "contact with the faceplate" and "sliding into the holes".
- **Surface Wiping.** The robot uses a whiteboard eraser to remove ink marks from the metallic surface of an unsecured microwave. As shown in Fig. 4 (d), it's hard to visually discern the contact state with wrist camera. The critical challenge is maintaining a precise force: the applied force must be sufficient to erase the ink ( $> 10\text{N}$ ) but low enough ( $< 25\text{N}$ ) to prevent the unsecured microwave from sliding away.
- **Dynamic Tossing.** The robot must pick up a piece of trash and toss it into a bin placed beyond its kinematic reach. This is a highly dynamic task where success depends on velocity preservation and precise release timing.
- **Conveyor Weight Sorting.** The robot must pick objects moving on a conveyor belt ( $v = 0.15\text{m/s}$ ) and place them into two distinct designated zones based on their weight, shown in Fig. 4 (e). The objects are visually identical but differ significantly in mass (Light: 50g vs. Heavy: 350g). The difficulty is twofold: (1) the policy must compensate for system latency to accurately track the moving target, and (2) it must infer the object's mass during the lifting phase to route the item to the correct target zone.

### 3) Data Collection: Adversarial Intervention Protocol.

As discussed in Sec. III-A, conditioning on history introduces the risk of *Causal confusion*, where the policy might spuriously correlate future actions with proprioceptive inertia rather than visual feedback. To mitigate this, we employ an *Adversarial Intervention Strategy* [17]. During data collection, a human supervisor actively perturbs the task environment—for example, shifting the target object or blocking the trajectory—while the operator attempts to perform the task. This forces the operator to generate recovery trajectories, creating a dataset

TABLE I: **Stiffness Characterization.** Effective stiffness  $k$  (N/m) and linearity ( $R^2$ ) across different axes and robot configurations.

Axis	Contracted Pose		Extended Pose		Change
	$k$ (N/m)	$R^2$	$k$ (N/m)	$R^2$	
X-axis (Longitudinal)	3501	0.981	2914	0.977	-17%
Y-axis (Lateral)	791	0.998	314	0.995	-60%
Z-axis (Vertical)	1709	0.977	328	0.992	-81%

distribution where proprioceptive history often contradicts the visual reality. This protocol ensures the learned policy acquires *Visual Grounding*, learning to rely on the Mismatch signal only when it aligns with the visual context.

**Human Strategy with Privileged Information.** Since our master interface is passive and lacks force feedback, a critical question arises: how does the human operator demonstrate force-sensitive or proprioceptive behaviors (e.g., feeling contact or weight) without direct force sensing? We clarify that the operator relies on privileged context during data collection to close the control loop:

- **Visual Proxy for Contact:** In tasks like Blind Plug Insertion and Wiping, the operator utilizes side-views to visually infer contact state.
- **Prior Knowledge of Weight:** In Conveyor Weight Sorting, the operator is informed of the object's mass beforehand and deliberately routes the object to the correct zone.

Crucially, this privileged information is withheld from the policy during training. The learning objective, therefore, implicitly forces the policy to discover the Intent-Execution Mismatch as the specific proprioceptive proxy that correlates with these high-level decisions. In essence, the model distills the human's visual and cognitive privileges into a proprioceptive representation.

### B. Result

1) **Validation of Monotonic Impedance (Q1):** To validate the *Monotonic Impedance Assumption*, we conducted a controlled indentation test using a high-precision digital scale. We recorded the ground-truth interaction force against the Intent-Execution Mismatch magnitude  $\|\epsilon_t\|$  across varying axes ( $x, y, z$ ) and workspace configurations.

**High-Fidelity Linear Proxy.** As shown in Fig. 5 and TABLE I, the relationship between mismatch and force yields

TABLE II: **Manipulation Capability Analysis.** We report success rates across four tasks. For the long-horizon Microwave task, we report the success rate for each stage (Open, Grasp, Place, Close) to diagnose different failure modes. For the Wiping task, we report both Strict Success (100% erased) and Effective Rate (residue < 50%)

Arch.	Method	Microwave Sequence				Plug (Clear)	Plug (Blind)	Wiping	
		Open	Grasp	Place	Close			Success	Effective
Diffusion Policy	S2S	0/20	11/20	15/20	14/20	-	-	0/20	0/20
	S2M	14/20	11/20	12/20	12/20	-	-	4/20	9/20
	<b>SM2M (Ours)</b>	<b>20/20</b>	12/20	17/20	<b>20/20</b>	-	-	13/20	17/20
$\pi_0$	S2S	0/20	<b>19/20</b>	17/20	13/20	0/20	0/20	0/20	0/20
	S2M	18/20	18/20	<b>20/20</b>	18/20	<b>19/20</b>	8/20	4/20	13/20
	<b>SM2M (Ours)</b>	<b>20/20</b>	<b>19/20</b>	<b>20/20</b>	<b>19/20</b>	<b>19/20</b>	<b>16/20</b>	<b>18/20</b>	<b>20/20</b>

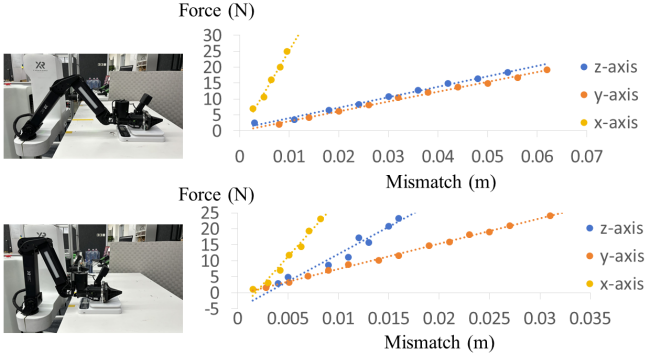


Fig. 5: **Validation of Monotonic Impedance (Q1).** We characterize the relationship between Intent-Execution Mismatch ( $\epsilon$ ) and ground-truth interaction Force across two distinct workspace configurations: (Down) Contracted Pose and (Up) Extended Pose.

high coefficients of determination ( $R^2 > 0.95$ ) across all test cases. This confirms that despite the black-box nature of the controller, the system behaves locally as a near-ideal spring ( $F \approx k\|\epsilon_t\|$ ), validating the mismatch signal as a high-fidelity proxy for force.

**Stiffness Anisotropy.** Crucially, while locally linear, the effective stiffness  $k$  varies drastically depending on the kinematic configuration. This variation is theoretically governed by the manipulator Jacobian ( $K_x \approx J^{-T} K_g J^{-1}$ ). Our learning-based approach implicitly captures this kinematic transformation directly from data, enabling precise force control without requiring an accurate URDF (Unified Robot Description Format) or explicit system identification.

2) **Force Generation (Q2):** To answer Q2, we analyze the performance gap between S2S and S2M. As shown in Table II, S2S fails across all contact-rich tasks. Validating our theoretical analysis in Sec. III-A, the S2S policy exhibits *force-agnostic* behavior: it accurately tracks geometry but fails to compensate for the system’s *finite stiffness*. This leads to specific physical failures:

- **Grasp Instability (Plug Task):** For rigid objects like plugs, the measured gripper width equals the object width. S2S clones this *zero-margin* state. Upon contact, the lack of command deviation results in insufficient

normal force to generate friction ( $F_{grasp} \approx 0$ ), causing the plug to slip.

- **Steady-State Error (Microwave Open Task):** Pressing the stiff button ( $\approx 10N$ ) creates a substantial reaction force. Due to the robot’s finite loop gain, the S2S policy—which targets the surface position—suffers from a *steady-state error*, stopping short of the trigger depth required to actuate the mechanism.
- **Loss of Sustained Contact (Wiping Task):** S2S policies, restricted to kinematic tracking, tend to “float” over the board. They trace the 2D cleaning pattern accurately but fail to exert the normal force required to erase the ink.

**Implicit Stiffness Modulation via Intent (S2M).** S2M effectively learns to modulate impedance by predicting the Master Intent. In grasping, it predicts a fully closed gripper; in insertion, it predicts compliant alignment. Crucially, for tasks requiring normal force, S2M learns to command a *Virtual Equilibrium Point* that penetrates the surface—such as commanding a position deep inside the button. This intentional mismatch forces the underlying position controller to eliminate the steady-state error and generate the necessary contact pressure.

**Remark on Controller Gains.** One might argue that S2S could succeed by strictly increasing the low-level controller gains ( $K_p$ ). However, this creates a *stiffness-compliance trade-off*. While high gains might enable button pressing, they render the policy dangerously rigid for tasks like Plug Insertion, where compliance is essential to resolve misalignment without jamming. S2M effectively bypasses this trade-off by learning a *task-dependent impedance* strategy on top of a moderate-gain controller.

3) **Force Perception (Q3):** While Intent Cloning (S2M) generates impedance, it remains an *open-loop* controller. SM2M closes the loop by utilizing mismatch history to perceive interaction dynamics. We validate this capability across three scenarios:

**Plug Insertion (Blind).** In the blind insertion task, the primary challenge is determining *when* to transition from search to insertion. Although S2M exhibits search patterns, it lacks the tactile feedback to confirm alignment. As shown in Table II, it achieves only 8/20 success. Qualitative analysis reveals that S2M often commits to the high-force insertion phase while still misaligned with the faceplate. This *premature*

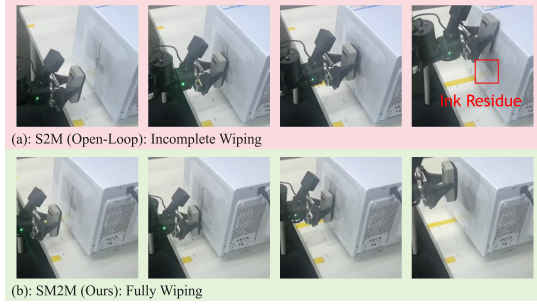


Fig. 6: **Qualitative Analysis of Force Perception in Wiping Task.** (a) S2M tracks the trajectory but lacks force feedback, resulting in ink residue due to insufficient pressure. (b) SM2M (Ours) utilizes mismatch history to implicitly regulate contact force, achieving clean erasure.

TABLE III: **Dynamic Manipulation Capability.** We report the success rates for Conveyor Weight Sorting (decomposed into Grasp, Place, Sort stages) and Dynamic Tossing tasks.

Model	Inference	Conveyor Weight Sorting			Tossing
		Grasp	Place	Sort	
<i>Diffusion Policy (DP)</i>					
S2S	Naïve Async	36 / 50	33 / 36	17 / 33	-
S2M	Naïve Async	44 / 50	36 / 44	20 / 36	-
<b>SM2M</b>	Naïve Async	<b>46 / 50</b>	<b>46 / 46</b>	<b>41 / 46</b>	-
<i><math>\pi_0</math> (Flow Matching)</i>					
SM2M	Sync	0 / 50	-	-	14 / 20
S2S	Naïve Async	35 / 50	32 / 35	16 / 32	17 / 20
S2M	Naïve Async	46 / 50	45 / 46	28 / 45	17 / 20
<b>SM2M</b>	Inpainting	<b>50 / 50</b>	<b>49 / 50</b>	<b>48 / 49</b>	<b>18 / 20</b>

insertion leads to jamming or causes the plug to slip within the gripper. SM2M utilizes the mismatch history to distinguish between “rigid contact” (hitting the faceplate) and “compliance” (sliding into the hole). This enables it to synchronize the insertion force with the geometric alignment, effectively preventing jamming.

**Surface Wiping.** Effective surface wiping requires a specific coordination strategy: establish normal force first, then initiate lateral motion. As shown in Table II, S2M achieves a high *Effective Rate* (13/20) but a low *Strict Success* (4/20). Qualitative analysis in Fig. 6 reveals that S2M often missing spots or moving too fast to ensure total erasure. SM2M (18/20) captures the human operator’s *press-then-move* strategy. By conditioning on the mismatch, the policy learns to wait until a sufficient vertical mismatch (proxy for normal force) is accumulated before executing the lateral cleaning pattern, ensuring consistent wiping pressure.

**Conveyor Weight Sorting.** As shown in Table III, since the light and heavy objects are visually identical (Fig. 1), both S2S and S2M fail to classify them correctly, performing near random guessing (Success Rate of Sort  $\approx$  50%). SM2M achieves near-perfect sorting (48/49) by inferring mass via tracking lag. As visualized in Fig. 7, heavy objects induce significantly larger vertical mismatch peaks ( $\epsilon_z$ ) during the lifting phase compared to light ones, providing a clear proprioceptive signal

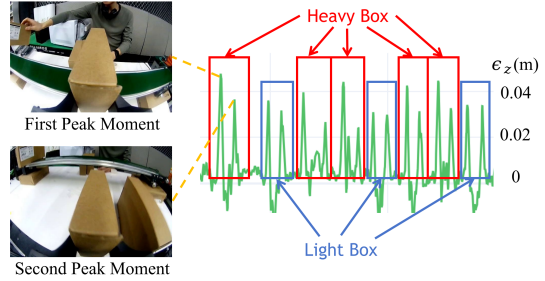


Fig. 7: **Mismatch in Conveyor Sorting Task.** We visualize the vertical Intent-Execution Mismatch ( $\epsilon_z$ ) during consecutive Conveyor Weight Sorting task. Heavy boxes (Red regions) induce significantly larger mismatch peaks during the lifting phase (First Peak Moment) compared to Light boxes (Blue regions).

TABLE IV: **Impact of Inference Latency.** We report the Success Rate and Motion Jerk ( $m/s^3$ ) in Conveyor Weight Sorting Task under artificial inference delays ranging from 100ms to 400ms.

Architecture	100 ms		200 ms		300 ms		400 ms	
	Succ	Jerk	Succ	Jerk	Succ	Jerk	Succ	Jerk
Naïve Async	50/50	0.75	47/50	0.80	45/50	1.01	40/50	1.28
<b>Ours</b>	50/50	0.75	48/50	0.78	48/50	0.82	45/50	0.88

for routing.

These results validate that the Intent-Execution Mismatch serves as a critical proprioceptive signal. It enables the policy to close the control loop, regulating force timing (Plug), synchronizing force with motion (Wiping), and inferring hidden physical properties (Sorting).

**4) Dynamic Capability and Latency Robustness (Q4):** To answer Q4, we first evaluate dynamic capability in Table III. The *Synchronous* baseline ( $\pi_0$  Sync) fails catastrophically on the Conveyor task (0/50 Grasp success rate) as the robot “freezes” during inference while targets move out of reach. Similarly, in Tossing, blocking inference interrupts momentum, reducing success to 14/20. Our Inpainting approach resolves this, achieving the highest stability (18/20) by ensuring  $C^1$  continuity.

We further stress-test robustness under artificial delays (100-400ms) in Table IV. While *Naïve Async* restores reactivity, it suffers from severe motion discontinuity at high latency, evidenced by a sharp rise in Jerk ( $0.75 \rightarrow 1.28 m/s^3$ ). In contrast, by explicitly conditioning on the committed action history to bridge the inference gap, our *Latency-Adaptive Inpainting* maintains smooth control ( $\text{Jerk} \approx 0.88 m/s^3$ ) and high success (45/50) even under worst-case delays.

## V. CONCLUSION

In this work, we argue that the fragility of current visuomotor policies on low-cost hardware stems from a fundamental misalignment between the learning objective and the physical reality of teleoperation. By shifting the paradigm from Exe-

cution Cloning to Intent Cloning, we bridge the gap between the robot’s compliant nature and the task’s physical demands.

Our framework systematically addresses three critical gaps in sensorless manipulation. First, we show that predicting the Master Intent allows the policy to function as an implicit impedance controller, generating the “Virtual Equilibrium Points” necessary to penetrate stiff constraints without explicit force control. Second, we demonstrate that the Intent-Execution Mismatch is a rich proprioceptive signal. By conditioning on this mismatch history, our policy distills the human operator’s privileged understanding of weight and friction into a learned sense of touch, enabling precise force modulation and physical property inference using only position encoders. Finally, we bridge the temporal gap via Latency-Adaptive Inpainting, ensuring robust dynamic tracking on moving conveyors where synchronous methods fail.

Ultimately, Mind the Gap presents a minimalist framework that empowers sensorless hardware to perform contact-rich and dynamic tasks.

## REFERENCES

- [1] Lars Ankile, Anthony Simeonov, Idan Shenfeld, Marcel Torne, and Pukit Agrawal. From Imitation to Refinement – Residual RL for Precise Assembly, 2024. URL <https://arxiv.org/abs/2407.16677>.
- [2] Kevin Black, Yecheng Jason Ma, William Paul, Anant Rai, Haresh Karnan, Alex X. Lee, Quan Vuong, Ted Xiao, Dorsa Sadigh, and Sergey Levine.  $\pi_0$ : A Vision-Language-Action Flow Model for General Robot Control. 2024. doi: 10.48550/arXiv.2410.24164. URL <https://arxiv.org/abs/2410.24164>.
- [3] Anthony Brohan et al. RT-2: Vision-Language-Action Models Transfer Web Knowledge to Robotic Control. In *Conference on Robot Learning*, 2023. doi: 10.48550/arXiv.2307.15818. URL <https://arxiv.org/abs/2307.15818>.
- [4] Lili Chen, Kevin Lu, Aravind Rajeswaran, Kimin Lee, Aditya Grover, Michael Laskin, Pieter Abbeel, Aravind Srinivas, and Igor Mordatch. Decision Transformer: Reinforcement Learning via Sequence Modeling, 2021. URL <https://arxiv.org/abs/2106.01345>.
- [5] Wendi Chen, Han Xue, Yi Wang, Fangyuan Zhou, Jun Lv, Yang Jin, Shirun Tang, Chuan Wen, and Cewu Lu. ImplicitRDP: An End-to-End Visual-Force Diffusion Policy with Structural Slow-Fast Learning, 2025. URL <https://arxiv.org/abs/2512.10946>.
- [6] Cheng Chi, Siyuan Feng, Yilun Du, Zhenjia Xu, Eric Cousineau, Benjamin Burchfiel, and Shuran Song. Diffusion policy: Visuomotor policy learning via action diffusion. In *Robotics: Science and Systems*, 2023. doi: 10.48550/arXiv.2303.04137. URL <https://arxiv.org/abs/2303.04137>.
- [7] Cheng Chi, Zhenjia Xu, Chuer Pan, Eric Cousineau, Benjamin Burchfiel, Siyuan Feng, Russ Tedrake, and Shuran Song. Universal Manipulation Interface: In-The-Wild Robot Teaching Without In-The-Wild Robots, 2024. URL <https://arxiv.org/abs/2402.10329>.
- [8] Open X-Embodiment Collaboration et al. Open x-embodiment: Robotic learning datasets and rt-x models. *arXiv preprint arXiv:2310.08864*, 2023. doi: 10.48550/arXiv.2310.08864. URL <https://arxiv.org/abs/2310.08864>.
- [9] Zipeng Fu, Tony Z. Zhao, and Chelsea Finn. Mobile ALOHA: Learning Bimanual Mobile Manipulation with Low-Cost Whole-Body Teleoperation, 2024. URL <https://arxiv.org/abs/2401.02117>.
- [10] Tomoya Fukuda, Masato Kobayashi, Yuki Uranishi, and Haruo Takemura. Bi-ACT: Bilateral Control-Based Imitation Learning via Action Chunking with Transformer. *arXiv preprint arXiv:2401.17698*, 2024. doi: 10.48550/arXiv.2401.17698. URL <https://arxiv.org/abs/2401.17698>.
- [11] Noah Geiger, Tamim Asfour, Neville Hogan, and Johannes Lachner. Diffusion-Based Impedance Learning for Contact-Rich Manipulation Tasks, 2025. URL <https://arxiv.org/abs/2509.19696>.
- [12] Ashish Kumar, Zipeng Fu, Deepak Pathak, and Jitendra Malik. RMA: Rapid Motor Adaptation for Legged Robots, 2021. URL <https://arxiv.org/abs/2107.04034>.
- [13] Seungjae Lee, Yibin Wang, Harietheja Etukuru, H. Jin Kim, Nur Muhammad Mahi Shafiqullah, and Lerrel Pinto. Behavior Generation with Latent Actions. In Ruslan Salakhutdinov, Zico Kolter, Katherine Heller, Adrian Weller, Nuria Oliver, Jonathan Scarlett, and Felix Berkenkamp, editors, *Proceedings of the 41st International Conference on Machine Learning*, volume 235 of *Proceedings of Machine Learning Research*, pages 26991–27008. PMLR, 21–27 Jul 2024. URL <https://proceedings.mlr.press/v235/lee24y.html>.
- [14] Yuki Namekawa et al. ILBiT: Imitation Learning for Robot Using Position and Torque Information based on Bilateral Control with Transformer. *arXiv preprint arXiv:2401.16653*, 2024. doi: 10.48550/arXiv.2401.16653. URL <https://arxiv.org/abs/2401.16653>.
- [15] Aaditya Prasad, Kevin Lin, Jimmy Wu, Linqi Zhou, and Jeannette Bohg. Consistency Policy: Accelerated Visuomotor Policies via Consistency Distillation, 2024. URL <https://arxiv.org/abs/2405.07503>.
- [16] Yuzhe Qin, Wei Yang, Binghao Huang, Karl Van Wyk, Hao Su, Xiaolong Wang, Yu-Wei Chao, and Dieter Fox. AnyTeleop: A General Vision-Based Dexterous Robot Arm-Hand Teleoperation System, 2024. URL <https://arxiv.org/abs/2307.04577>.
- [17] Stéphane Ross, Geoffrey J Gordon, and J Andrew Bagnell. A reduction of imitation learning and structured prediction to no-regret online learning. In *Proceedings of the fourteenth international conference on artificial intelligence and statistics*, pages 627–635, 2011. doi: 10.48550/arXiv.1011.0686. URL <https://proceedings.mlr.press/v15/ross11a.html>.

- [18] Yuki Sasagawa, Sho Sakaino, and Toshiaki Tsuji. Motion generation using bilateral control-based imitation learning with autoregressive learning. *IEEE Access*, 9:20508–20520, 2021. doi: 10.1109/access.2021.3054960. URL <https://doi.org/10.1109/access.2021.3054960>.
- [19] Nur Muhammad Mahi Shafiullah, Zichen Jeff Cui, Ar-iuntuya Altanzaya, and Lerrel Pinto. Behavior Transformers: Cloning  $k$  modes with one stone, 2022. URL <https://arxiv.org/abs/2206.11251>.
- [20] Octo Model Team, Dibya Ghosh, Homer Walke, Karl Pertsch, Kevin Black, Oier Mees, Sudeep Dasari, Joey Hejna, Tobias Kreiman, Charles Xu, Jianlan Luo, You Liang Tan, Lawrence Yunliang Chen, Pannag Sanketi, Quan Vuong, Ted Xiao, Dorsa Sadigh, Chelsea Finn, and Sergey Levine. Octo: An Open-Source Generalist Robot Policy, 2024. URL <https://arxiv.org/abs/2405.12213>.
- [21] Chikaha Tsuji, Enrique Coronado, Pablo Osorio, and Gentiane Venture. Adaptive Contact-Rich Manipulation Through Few-Shot Imitation Learning With Force-Torque Feedback and Pre-Trained Object Representations. *IEEE Robotics and Automation Letters*, 10(1):240–247, 2025. URL <https://ieeexplore.ieee.org/abstract/document/10752344>.
- [22] Han Xue, Jieji Ren, Wendi Chen, Gu Zhang, Yuan Fang, Guoying Gu, Huazhe Xu, and Cewu Lu. Reactive Diffusion Policy: Slow-Fast Visual-Tactile Policy Learning for Contact-Rich Manipulation, 2025. URL <https://arxiv.org/abs/2503.02881>.
- [23] Jiawen Yu, Hairuo Liu, Qiaojun Yu, Jieji Ren, Ce Hao, Haitong Ding, Guangyu Huang, Guofan Huang, Yan Song, Panpan Cai, Cewu Lu, and Wenqiang Zhang. ForceVLA: Enhancing VLA Models with a Force-aware MoE for Contact-rich Manipulation, 2025. URL <https://arxiv.org/abs/2505.22159>.
- [24] Zongzheng Zhang, Haobo Xu, Zhuo Yang, Chenghao Yue, Zehao Lin, Huan ang Gao, Ziwei Wang, and Hao Zhao. TA-VLA: Elucidating the Design Space of Torque-aware Vision-Language-Action Models, 2025. URL <https://arxiv.org/abs/2509.07962>.
- [25] Tony Z Zhao, Vikash Kumar, Sergey Levine, and Chelsea Finn. Learning fine-grained bimanual manipulation with low-cost hardware. In *Proceedings of Robotics: Science and Systems*, 2023. doi: 10.15607/RSS.2023.XIX.016. URL <https://arxiv.org/abs/2304.13705>.

## APPENDIX A TASK DETAILS

In this section, we provide a detailed breakdown of each manipulation task and analyze the correspondence between the physical execution stages and the recorded *Intent-Execution Mismatch* ( $\epsilon_t = \mathbf{x}_t^m \ominus \mathbf{x}_t^s$ ). The mismatch curves are plotted in the local robot base frame: X-axis (Forward), Y-axis (Left), and Z-axis (Up).

As illustrated in Fig. 8, each task is decomposed into key semantic stages (e.g., Push Button, Aligning, Wiping). The corresponding mismatch curves demonstrate that  $\epsilon_t$  is not random noise, but a rich, informative signal that varies consistently with the task dynamics.

We highlight three key physical phenomena encoded in these signals across different tasks:

- **Dynamic Compensation in Free Space Motion:** Contrary to the intuition that mismatch arises solely from contact, significant fluctuations in  $\epsilon$  are observed during rapid free-space motion (e.g., the Start phase). This indicates that the policy learns to lead the robot, generating a mismatch that compensates for system inertia and tracking lag to achieve the desired acceleration.
- **Implicit Force Regulation:** In contact-rich stages, such as Pushing the Button (Fig. 8 (a)) or Wiping Surface (Fig. 8 (e)), the mismatch often stabilizes into a sustained non-zero offset. For example, a constant positive  $\epsilon_x$  during wiping represents a Virtual Equilibrium Point below the surface, acting as a proxy for normal force to maintain contact pressure.
- **Physical Property Inference:** The mismatch signal acts as a proprioceptive sensor for system identification. In the Conveyor Weight Sorting task (Fig. 8 (d)), lifting a Heavy object induces a significantly larger mismatch peak compared to a Light object due to gravity and payload inertia. The policy conditions on this history to infer object mass and route it to the correct bin.

## APPENDIX B

### MODEL ARCHITECTURE AND IMPLEMENTATION DETAILS

In this section, we provide the implementation specifics of the Dual-State Conditioning framework and the Latency-Adaptive Inpainting mechanism. We detail how we adapt standard backbone architectures—specifically Diffusion Policy (DP) [3] and  $\pi_0$  [1]—to incorporate the Intent-Execution Mismatch and handle inference latency.

#### A. Input Representation: Dual-State Conditioning

**Coordinate Reference Frames.** The pose of each robotic arm (both Master and Slave) is represented in its respective Local Base Frame (the fixed coordinate system attached to the mounting base of each manipulator). For the bimanual Microwave task, the left and right arms operate in independent coordinate systems. We do not perform extrinsic calibration to unify them into a common global frame; instead, the policy implicitly learns the spatial coordination between the two independent base frames from the demonstration data. The

pose  $\mathbf{x} \in \mathbb{R}^7$  consists of translation  $(x, y, z)$ , Euler angles  $(r, p, y)$ , and gripper width. Note that these are **absolute poses** relative to the local base.

**Input Modalities and Temporal Structure.** The input configuration is strictly tailored to the task requirements. For the bimanual **Microwave** task, the policy conditions on visual observations from three RGB streams (left wrist, right wrist, and first-person view). The proprioceptive input is constructed by concatenating the states of all four arm components—Slave Left, Slave Right, Master Left, and Master Right—resulting in a unified **28-dimensional** vector. In contrast, for all single-arm tasks (**Plug**, **Wiping**, **Tossing**, **Sorting**), the input is streamlined to a single wrist-mounted camera view and a **14-dimensional** proprioceptive vector formed by concatenating the single-arm Slave and Master states. Crucially, we decouple the temporal observation horizons for these modalities: while visual features are extracted strictly from the **current frame** ( $T_{img} = 1$ ) to minimize computational load, proprioceptive states are ingested as a **history sequence** ( $T_{state} \geq 1$ ) to provide essential dynamic context for force perception without the overhead of video processing.

**Robustness to Task-Irrelevant Inputs.** During initial pilot experiments, we observed that including task-irrelevant modalities, such as adding the left-arm state or secondary camera views to single-arm manipulation tasks, led to a measurable degradation in success rates. We attribute this to the model attempting to identify spurious correlations within these high-dimensional nuisance variables. Consequently, our framework adopts a minimalist design principle: we explicitly tailor the input observation space to the specific degrees of freedom and visual field required for each task. This ensures that the policy focuses exclusively on the relevant inputs, maximizing robustness and sample efficiency on low-cost hardware.

#### B. Backbone Architecture Modifications

**Adaptation for  $\pi_0$  (Flow Matching).** For the  $\pi_0$  architecture, which utilizes a Transformer backbone, we treat each timestep of the trajectory as a single input token. To align with the pre-trained embedding layer which expects a fixed dimension of  $D = 32$ , we zero-pad the unified 14-dimensional or 28-dimensional proprioceptive vectors defined above to the required size. A critical implementation detail lies in constructing tokens for the *Committed Intent* (the future Master trajectory fixed by the inpainting mask). Since the future Slave execution is unknown at inference time, we explicitly construct these future tokens by concatenating the future Master state with the current Slave state during both training and inference. This formulation allows the Transformer to condition on the precise future intent while effectively informing the model that the robot has not yet physically reacted to these upcoming commands.

**Adaptation for Diffusion Policy (DP).** We utilize the standard CNN-based 1D Temporal U-Net as our backbone. To implement *Latency-Adaptive Inpainting*, we modify the input to the noise prediction network by channel-wise concatenating the noisy action  $\mathbf{A}_{t+1:t+H}$  (where  $H$  denotes the prediction

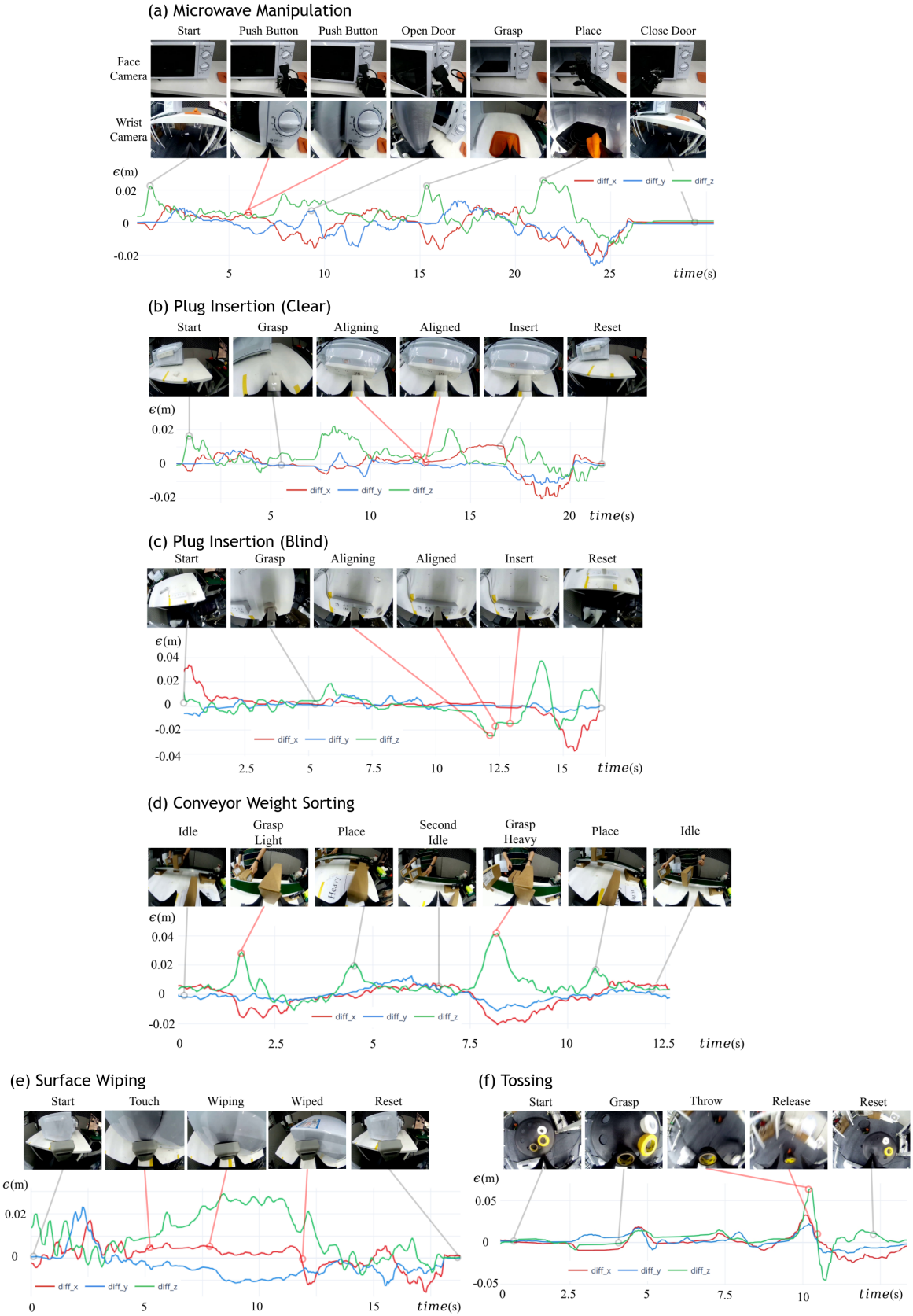


Fig. 8: Task Frames and Mismatch Visualization for All Task

horizon), the committed intent  $\mathbf{X}_{cond}^m$ , and the binary validity mask  $\mathbf{M} \in \{0, 1\}^H$ . Crucially,  $\mathbf{X}_{cond}^m$  is constructed by taking the committed trajectory for the first  $k$  steps and *padding the remaining  $H - k$  steps with the last committed state  $\mathbf{x}_{t+k}^m$* . This ensures the network receives a continuous guidance signal rather than zero-filled voids. Furthermore, we employ *asymmetric observation horizons*: the visual encoder processes only the current frame ( $T_{img} = 1$ ) to minimize latency, while the proprioceptive encoder receives a history window ( $T_{obs}$ ) of dual-state vectors  $[\mathbf{x}^m, \mathbf{x}^s]$  to capture high-frequency mismatch dynamics.

### C. Training Objective and Inference Execution

**Minimalist Backbone Integration.** We emphasize that our framework relies solely on input conditioning, requiring **no modifications** to the core training objectives, loss functions, or the internal sampling dynamics (e.g., noise scheduling or inference sampler) of the backbone models. For both Diffusion Policy (utilizing standard MSE loss with DDIM scheduling) and  $\pi_0$  (utilizing the standard Flow Matching objective with ODE solvers), the optimization targets remain invariant. This alignment ensures that our Dual-State Conditioning framework serves as a plug-and-play module, easily integrated into existing robot learning pipelines by simply modifying the input encoder without the need to alter the underlying generative mechanics.

**Latency-Aware Execution Strategy.** During inference, the policy predicts a full action chunk of length  $T_{pred}$ . However, due to the non-zero inference latency  $\delta_{inf}$ , the first  $k = \lceil \delta_{inf}/\Delta t \rceil$  steps of the prediction correspond to the time interval that has already elapsed during computation. We **discard** these first  $k$  steps and execute the trajectory starting from step  $k + 1$ . In the context of our Inpainting framework, these discarded steps correspond precisely to the “Committed Intent” used as input conditioning.

## APPENDIX C

### TRAINING DETAILS AND HYPERPARAMETER ANALYSIS

In this section, we provide the training protocols and a detailed analysis of the hyperparameter choices. We specifically discuss the trade-off between history length and causal confusion in contact-rich manipulation.

#### A. Experimental Setup and Hyperparameters

All models were trained on a single **NVIDIA A100 (80GB) GPU**. The training configuration is standardized across tasks to ensure fair comparison, with specific variations only in the observation history and inference strategy to accommodate task dynamics.

The detailed hyperparameters, primarily based on the  $\pi_0$  configuration, are listed in Table V.

#### B. Hyperparameter Analysis

**The Risk of Causal Confusion ( $T_{obs}$ ).** A key finding in our experiments is that “more history is not always better.”

- **Quasi-Static Tasks ( $T_{obs} = 1$ ):** For tasks like *Surface Wiping* or *Plug Insertion*, the interaction force is

TABLE V: Standardized Training Hyperparameters

Category	Value / Setting
<i>Optimization</i>	
Optimizer	AdamW ( $\beta_1 = 0.9, \beta_2 = 0.95$ )
Peak Learning Rate	$2.5e^{-5}$
LR Schedule	Warmup (1,000 steps) + Cosine Decay
Weight Decay	$1e^{-10}$
Batch Size	16
Training Steps	30,000
<i>Common Prediction Parameters</i>	
Prediction Horizon ( $T_{pred}$ )	30 steps
Execution Horizon ( $T_{exec}$ )	15 steps
Visual Input ( $T_{img}$ )	1 (Current Frame Only)
<i>Task-Specific Variations</i>	
<b>Quasi-Static Tasks</b> (Microwave, Plug, Wipe)	$T_{obs} = 1$ , Inference: <i>Synchronous</i>
<b>Dynamic Tasks</b> (Sorting, Tossing)	$T_{obs} = 9$ , Inference: <i>Inpainting</i>

physically determined by the *instantaneous* mismatch ( $F \propto k\epsilon_t$ ). We found that conditioning on a long history ( $T_{obs} = 9$ ) degraded success rates. We attribute this to **Causal Confusion**: the model learns spurious correlations between future actions and past trajectory trends rather than reacting to the immediate geometric constraints. Therefore, we strictly limit  $T_{obs} = 1$  for these tasks to force the policy to function as an instantaneous impedance controller.

- **Dynamic Tasks ( $T_{obs} = 9$ ):** In contrast, for *Weight Sorting*, the instantaneous state is insufficient to distinguish object mass. The policy requires a temporal window to integrate the mismatch signal for implicit system identification. Thus, we use  $T_{obs} = 9$  solely for dynamic tasks.

**Action Execution Horizon ( $T_{exec}$ ).** The execution horizon determines the open-loop control duration before replanning. Our pilot studies revealed that high-precision tasks (e.g., *Blind Plug Insertion*) benefit from a shorter horizon ( $T_{exec} \approx 10$ ) to maximize replanning frequency and tactile reactivity. In contrast, friction-heavy tasks (e.g., *Wiping*) benefit from a longer horizon ( $T_{exec} \approx 20$ ) to prevent freezing (stagnation) by committing to smoother, longer motion chunks. Despite these task-specific optima, we selected a unified  $T_{exec} = 15$  in all reported benchmarks for a fair comparison. Besides, we perform  $3\times$  temporal interpolation on the predicted action chunk. The standardized execution horizon of  $T_{exec} = 15$  model steps corresponds to a physical duration of 0.75 seconds in 60Hz control frequency.

## APPENDIX D

### FAILURE ANALYSIS

We analyze the failure modes to highlight the specific roles of Force Generation (Intent Clone) and Force Perception (Mismatch Aware). Fig. 9 visually contrasts the force deficit of the baseline (S2S) with the perception deficit of the open-loop Intent Cloning (S2M).

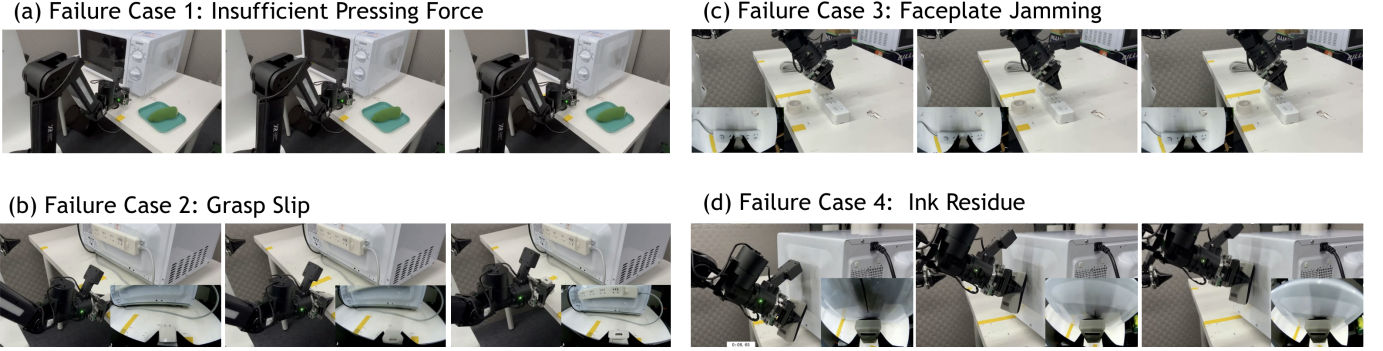


Fig. 9: Failure Cases in different tasks.

**(a) Button Press Failure (S2S, Microwave).** *Failure of Force Generation.* The S2S policy accurately tracks the geometric trajectory but halts exactly at the button surface. Lacking the virtual penetration intent, it fails to generate the activation force ( $\approx 10\text{N}$ ), causing the robot to freeze at the button.

**(b) Grasp Slip (S2S, Plug Clear).** *Failure of Grip Force.* By cloning the *measured* gripper width, the S2S policy outputs a zero-margin command. This results in negligible clamping force, causing the rigid plug to slip or rotate during transport.

**(c) Faceplate Jamming (S2M, Plug Blind).** *Failure of Contact Perception.* While S2M generates sufficient insertion force, it operates open-loop. It cannot distinguish between “sliding into the hole” and “hitting the faceplate”. Consequently, it often commits to a high-force insertion while misaligned, leading to jamming against the rigid surface rather than correcting its pose.

**(d) Ink Residue (S2M, Wiping).** *Failure of Force Regulation.* Effective surface wiping requires a specific coordination strategy: establish normal force first, then initiate lateral motion. S2M often misses spots or moves too fast to ensure total erasure.